RESEARCH PAPER

High levels of microRNA-21 in the stroma of colorectal cancers predict short disease-free survival in stage II colon cancer patients

Boye Schnack Nielsen · Stine Jørgensen · Jacob Ulrik Fog ·
Rolf Søkilde · Ib Jarle Christensen · Ulla Hansen ·
Nils Brünner · Adam Baker · Søren Møller · Hans Jørgen Nielsen

Abstract Approximately 25% of all patients with stage II colorectal cancer will experience recurrent disease and subsequently die within 5 years. MicroRNA-21 (miR-21) is upregulated in several cancer types and has been associated with survival in colon cancer. In the present study we developed a robust in situ hybridization assay using high-affinity Locked Nucleic Acid (LNA) probes that specifically detect miR-21 in formalin-fixed paraffin embedded (FFPE) tissue samples. The expression of miR-21 was analyzed by in situ hybridization on 130 stage II colon and 67 stage II rectal cancer specimens. The miR-21 signal was revealed as a blue chromogenic reaction, predominantly observed in fibroblast-like cells located in the stromal compartment of the tumors. The expression levels were measured using image analysis. The miR-21 signal was determined as the total blue area (TB), or the area fraction relative to the nuclear density (TBR) obtained using a red nuclear stain. High TBR (and TB) estimates of miR-21 expression correlated significantly with shorter disease-free survival ($p = 0.004$, HR = 1.28, 95% CI: 1.06–1.55) in the stage II colon cancer patient group, whereas no significant correlation with disease-free survival was observed in the stage II rectal cancer group. In multivariate analysis both TB and TBR estimates were independent of other clinical parameters (age, gender, total leukocyte count, K-RAS mutational status and MSI). We conclude that miR-21 is primarily a stromal microRNA, which when measured by image analysis identifies a subgroup of stage II colon cancer patients with short disease-free survival.

Keywords MicroRNA · MiR-21 · Colorectal cancer · In situ hybridization · LNA

B. S. Nielsen (✉) · S. Jørgensen · J. U. Fog · R. Søkilde ·
A. Baker · S. Møller
Exiqon A/S, Diagnostic Product Development,
Skelstedet 16, 2950 Vedbaek, Denmark
e-mail: bosn@exiqon.com

I. J. Christensen
The Finsen Laboratory, Rigshospitalet, 2200 Copenhagen N,
Denmark

U. Hansen
Department of Pathology, Hvidovre Hospital,
2650 Hvidovre, Denmark

N. Brünner
Section of Pathobiology, Department of Veterinary Disease
Biology, Faculty of Life Sciences, University of Copenhagen,
Frederiksberg, Denmark

H. J. Nielsen
Department of Surgical Gastroenterology,
Hvidovre Hospital, 2650 Hvidovre, Denmark

Abbreviations

CC	Colon cancer
RC	Rectal cancer
CRC	Colorectal cancer
DIG	Digoxigenin
DFS	Disease-free survival
ISH	In situ hybridization
LCM	Laser capture microdissection
LNA	Locked nucleic acid
miRNA	microRNA
NBT	4-Nitro-blue tetrazolium
BCIP	5-Brom-4-chloro-3′-indolylphosphate

TB   Total blue area
TBR   Total blue area per nuclear red area

Introduction

Colorectal cancer (CRC) is the third most frequent cancer disease and the second most frequent cause of cancer related mortality in the Western World. There are approximately 600,000 new cases annually in these countries [1, 2]. In stage II CRC the tumor is confined to the bowel wall in contrast to stage III and IV, in which the tumors have disseminated to local lymph nodes and distant organs, respectively. Removal of primary stage II CRC is therefore intended to be curative; however, 20–25% of all stage II CRC patients will present with recurrent disease and subsequent death from the disease within 5 years after primary surgery. The majority of patients with stage II CRC do not receive adjuvant treatment since at present there is no evidence for a beneficial effect of systemic adjuvant treatment for this patient group as a whole [3].

MicroRNAs (miRNAs) constitute a group of 18–22 base-pair long non-coding RNAs. Some miRNA genes, including miR-21, are transcribed as long non-coding RNAs with polyadenylation [4]. miRNA biogenesis and activity is only partially understood, but a generally accepted sequence of steps is known as the "linear" canonical pathway [5].

miR-21 is consistently upregulated in a variety of cancer tissues including colon [6, 7], esophagus [8], gastric [9], lung [10], and breast cancer [11–15]. The human *miR-21* gene is located on chromosome 17q23-1 overlapping with the *TMEM49* gene, a human homologue of rat Vacuole Membrane Protein 1 *VMP-1* [4, 16]. *miR-21* encodes a single hairpin and is regulated by its own promoter containing binding sites for AP-1 and PU.1 transcription factors [16]. Several mRNAs have been identified as targets of miR-21 mediated regulation including PDCD4 [17, 18], SPRY1 and 2 [19, 20], NFI-B [16], RECK [21], and PTEN [22–24].

To better characterize the molecular pathways regulated by miR-21 in disease processes, determination of its cellular origin is crucial. In situ hybridization (ISH) analysis for miRNAs is a highly sensitive but technically challenging technology that is used to analyze miRNA localization and expression. The limited size of the miRNAs requires highly specific detection reagents. In studies of CRC tissues, ISH was utilized for cellular localization of miR-21, but they present diverging results. Schetter et al. [7] found miR-21 staining of an epithelial colon cancer (CC) cell sub-population only, whereas Yamamichi et al. [25] reported expression in both tumor cells and stromal

fibroblasts. In a recent study that included CRC samples the miR-21 ISH signal was also seen in both tumor and stromal cells [26]. In this study we have employed high affinity LNA-modified DNA probes together with a series of positive and negative control probes to show that miR-21 is predominantly located in stromal fibroblast-like cells within the tumor. We also developed an image analysis-based algorithm that allowed semi-quantitative assessment of the ISH signal in the clinical samples and show a significant correlation between high miR-21 levels and short disease-free survival in CC patients.

Materials and methods

Patients

This study included formalin-fixed paraffin embedded tumor specimens from 234 CRC patients [149 stage II (Dukes B) CC and 85 stage II rectal cancer (RC) patients], who were all part of the RANX05 study cohort [27]. The original RANX05 study, approved according to the local scientific-ethics committee for Københavns and Frederiksberg Kommuner KF-200.2045/91, included 274 stage II CRC patients in the Danish cohort. Not all departments provided tissue samples, which resulted in 238 samples listed for the current study. Four samples were not available resulting in a total of 234 samples. Hematoxylin and eosin (H&E) staining was performed on all 234 samples, and we noted that seven samples (2 CC and 5 RC) did not contain cancer tissue and these were therefore not processed for the ISH analysis. The remaining 227 tumor specimens contained both normal mucosa and tumor tissue. Of these an additional 30 samples (17 colon and 13 rectal tumors) had either a small tumor area (<20 mm^2) or experienced significant tissue damage or prevalent staining artifacts after ISH processing and were excluded in the statistical analysis. Patients within the RANX05 study underwent surgery for CRC during 1991–1993 and were followed for at least 60 months. None of the CC patients received adjuvant chemotherapy and none of the RC patients received radio- or chemotherapy. Patients who were categorized as having an event in the calculation of disease-free survival (DFS) experienced local tumor recurrence in the form of either local or distant metastasis, or death due to CRC, the latter obtained from the Danish Causes of Death Registry. Patients dying of all causes were considered as "death events" and were included as such in the overall survival (OS) analysis. Clinical data in addition to the follow-up data, included gender, age, differentiation grade (high, moderate or low), tumor type (adenocarcinomas, mucinous or signet ring carcinoma) according to the WHO classification, total leukocyte count [28], microsatellite instability

(MSI) [29], and K-RAS mutation status. Differentiation grade, tumor type determination, MSI status and K-RAS mutation status were obtained for CC, only.

LNA probes

DNA oligonucleotides with app. 30% Locked Nucleic Acid (LNA) substitutions [30] for full length miR-21 (the miRCURY^{TM} probe, predicted Tm $\sim$ 82.7°C, measured Tm $\sim$ 83.7°C to miR-21 RNA target sequence): tcaacatcagtctgataagcta (Exiqon, Vedbaek, Denmark). Two additional oligos for miR-21 were designed including a 17-mer at the 5′-end (acatcagtctgataagc, predicted Tm $\sim$ 82°C), and a 15-mer at the 3′-end (tcaacatcagtctga, predicted Tm $\sim$ 81°C). In addition, we prepared a 22-mer probe containing three mis-matches (tcatcaacactctgataagcta, predicted Tm $\sim$ 83°C to complementary RNA sequence, measured Tm $\sim$ 61°C to miR-21 RNA sequence). A probe specific for U6 snRNA (cacgaatttgcgtgtcatcctt, predicted Tm $\sim$ 84°C, Exiqon) was used as positive control, and a 22-mer scrambled probe with a random sequence (gtgtaacacgtctatacgccca, predicted Tm $\sim$ 87°C) having no known complementary sequence target among human transcripts performing MegaBLAST search at NCBI GenBank, was included as negative control. All LNA oligos were digoxigenin (DIG)-labeled at the 5′- and 3′-ends except the U6 probe, which was only 5′-end labeled, or if otherwise specified.

In situ hybridization

Six μm-thick paraffin sections were mounted on Super frost + glass slides and deparaffinized. The slides were mounted onto flow through slide chambers and placed in a Tecan Freedom Evo automated hybridization instrument (Tecan, Männedorf, Switzerland) in which the following steps were performed: proteinase-K treatment 15 μg/ml at 37°C for 8 min, pre-hybridization in Exiqon hybridization buffer (Exiqon, Vedbæk, Denmark) at 62°C for 15 min, hybridization with 40 nM miR-21 probe, stringent washes with 5 × SSC, 1 × SSC and 0.2 × SSC buffers at 62°C over 33 min, DIG blocking reagent (Roche, Mannheim, Germany) in maleic acid buffer containing 2% sheep serum at 30°C for 15 min, alkaline phosphatase-conjugated anti-digoxigenin (diluted 1:500 in blocking reagent, Roche) at 30°C for 30 min, enzymatic development using 4-nitro-blue tetrazolium (NBT) and 5-brom-4-chloro-3′-Indolyl-phosphate (BCIP) substrate (Roche) forming dark-blue NBT-formazan precipitate at 30°C for 60 min, nuclear fast red counterstain (Vector Laboratories, Burlingname, CA), at 25°C for 1 min. The slides were then dismantled in water, dehydrated in alcohol solutions and mounted with eukitt mounting medium (VWR, Herlev, Denmark). For

each patient, two slides were hybridized with the full length miR-21 probe. To minimize day–day variations all probes were pre-diluted in hybridization buffer in quantities determined for a single experiment. The same proteinase-K stock was used through-out the experimental period. The following steps were standardized in all steps on different experimental days: tissue sectioning at 6 μm, incubation times, incubation temperatures, pre-diluted probes, antibody dilutions, proteinase-K batch. For probe specificity analysis the full length miR-21 probe was replaced with the 5′-end probe, 3′-end probe, 3-mismatch probe, scrambled probe (all at 40 nM), or the probe for U6 snRNA (0.1 nM). For fluorescent ISH, the sections were processed as above, except that detection of the DIG-labeled probes was done with peroxidase-conjugated sheep anti-DIG (Roche) followed by TSA-FITC substrate (Invitrogen, Taastrup, Denmark) according to manufacturer's recommendations. Slides were coverslipped using DAPI mounting media (Invitrogen).

Image analysis and quantification

For image analysis we used the Visiopharm integrated microscope and software module (Visiopharm, Hørsholm, Denmark), comprising a Leica DM 6000B microscope (Leica, Herlev, Denmark) equipped with an automated stage and slide loader (Ludl, Hawthorne, USA) and an Olympus DP72 CCD camera. Overview images of tissue sections were captured using a 1.25× objective. The tumor area (20–40 mm^2) was encircled on the overview images in which 8–17 random image fields were collected using systematic uniform random area sampling. The sample images were captured with a 20× objective covering 0.29 mm^2 each. Exposure of sample images was strictly controlled and locked at 6.993 ms with RGB (red–green–blue) values at 170–180 in non-stained blank areas. Sample images with tissue and staining artifacts were excluded. All sample images included contained areas with evident cancer cells and tumor stroma. Sample image exclusion was done by an observer (BSN) unaware of the clinical parameters. We employed supervised segmentation based on Bayesian classification using the Visiomorph software tool. For miR-21 quantification, the following histologically stained structures were differentiated: blue areas (B) corresponding to the hybridization signal, red area (R) corresponding to the red nuclear stain, purple areas (P) corresponding to blue ISH signal overlaying nuclear red stain. In addition, mucinous secretion stained with NFR (mostly observed within normal mucosa and only sporadically appearing in cancer areas) could be discriminated and was considered as background signal. The following parameters were obtained for each sample image: B, R, P, total blue (TB = B + P), total red (TR = R + P), as well

as TBR = TB/TR. Minimal (less than 1%) mis-classification of the blue signal and no mis-classification with the red signal was observed when applying the pixel classifier to NFR stained sections with no NBT-formazan development and to NBT-BCIP stained sections with no NFR counter stain indicating that the classifier efficiently discriminated the blue NBT-formazan precipitate from the NFR stained nuclei (data not shown). Three parameters obtained from image analysis and reflecting relative miR-21 expression levels were considered: (1) the stained area, (2) the staining intensity and (3) the number of positive cells. Since the stromal cells were often overlapping we did not pursue a model based on numbers of positive cells. In our image analysis set-up we evaluated a measure of *ISH signal intensity* within the whole image field. These intensity values did not vary much and combining the intensity parameter with area measures did not improve the correlation of the area measure to survival. For determination of the intra-assay variation, we captured random images ($n = 7$) from six random slides three times. For these six slides, the average CV was found to be 94% for TBR and 84% for the TB value, thus the same range as the inter-slide variation that for all 197 cases were 67 and 71%, respectively (see p. 14).

Laser capture microdissection and RT-qPCR

5 μm-thick paraffin sections were fixed on PEN membrane frame slides (Molecular Devices, Sunnyvale, CA) and stained with Hematoxylin and Eosin. Tissue fractions ($50–200 \times 10^3$ μm^2) of normal adjacent mucosa, tumor stroma, and cancer cells were isolated into separate Cap-Sure® Macro LCM Caps (Molecular Devices) using an Arcturus Veritas Laser Capture Microdissection System (Molecular Devices). RNA was purified using the FFPE miRNeasy kit (Qiagen, Valencia, CA). RT-qPCR was performed using the miRCURY LNA™ Universal RT microRNA PCR system (Exiqon) on a Lightcycler-480 (Roche). Quantification cycle (Cq) was calculated using the 2nd derivative method. Melting curve analysis was performed to verify amplification of single PCR products.

Determination of microsatellite instability (MSI)

MSI was determined in DNA purified from 10 μm-thick paraffin sections by PCR for five markers as described [31]. Patients with MSI score 3–5 were considered MSI-positive.

K-RAS genotypin

K-RAS mutational status (wild type vs. mutation) was determined on the purified DNA obtained for the MSI analysis (above) using the Therascreen K-RAS mutation

qPCR kit (Qiagen/DxS, Manchester, UK) according to manufacturer's instructions. The qPCR analysis detects the presence of 7 K-RAS mutations: Gly12Asp (GGT > GAT), Gly12Ala (GGT > GCT), Gly12Val (GGT > GTT), Gly12Ser (GGT > AGT), Gly12Arg (GGT > CGT), Gly12Cys (GGT > TGT), and Gly13Asp (GGC > GAC). The presence of one or more of these mutations categorized the patient as positive in K-RAS mutational status.

Statistical analysis

All statistical calculations were performed using SAS (version 9.1). The level of significance was set to 5%. Variance components for the estimation of intra-individual variance and the inter-individual variance were done and the results presented by the coefficient of variation (CV) and the intra-class correlation coefficients (ICC). The Wilcoxon rank sum test was used to test for differences in levels between cases clinical parameters. DFS analysis was done using the Cox proportional hazards model and defined as local recurrence, distant metastases or death attributable to CRC (primary cause). Overall survival (OS) was defined as death due to any cause. Age and gender were included as baseline covariates. All analyses were stratified by localization. The miR-21 values (TB or TBR) were analyzed as continuous variables on the log scale (base 2). The estimated HR values are therefore representing a 2-fold increase in the miR-21 values. Model validation has been done for the proportional hazards assumption and linearity of the covariates. Kaplan–Meier estimates of DFS are presented with patients grouped by the tertiles of the miR-21 values with differences between strata tested using the log-rank statistic. The assumption of linearity and the proportional hazards assumption were assessed using Schoenfeld and martingale residuals.
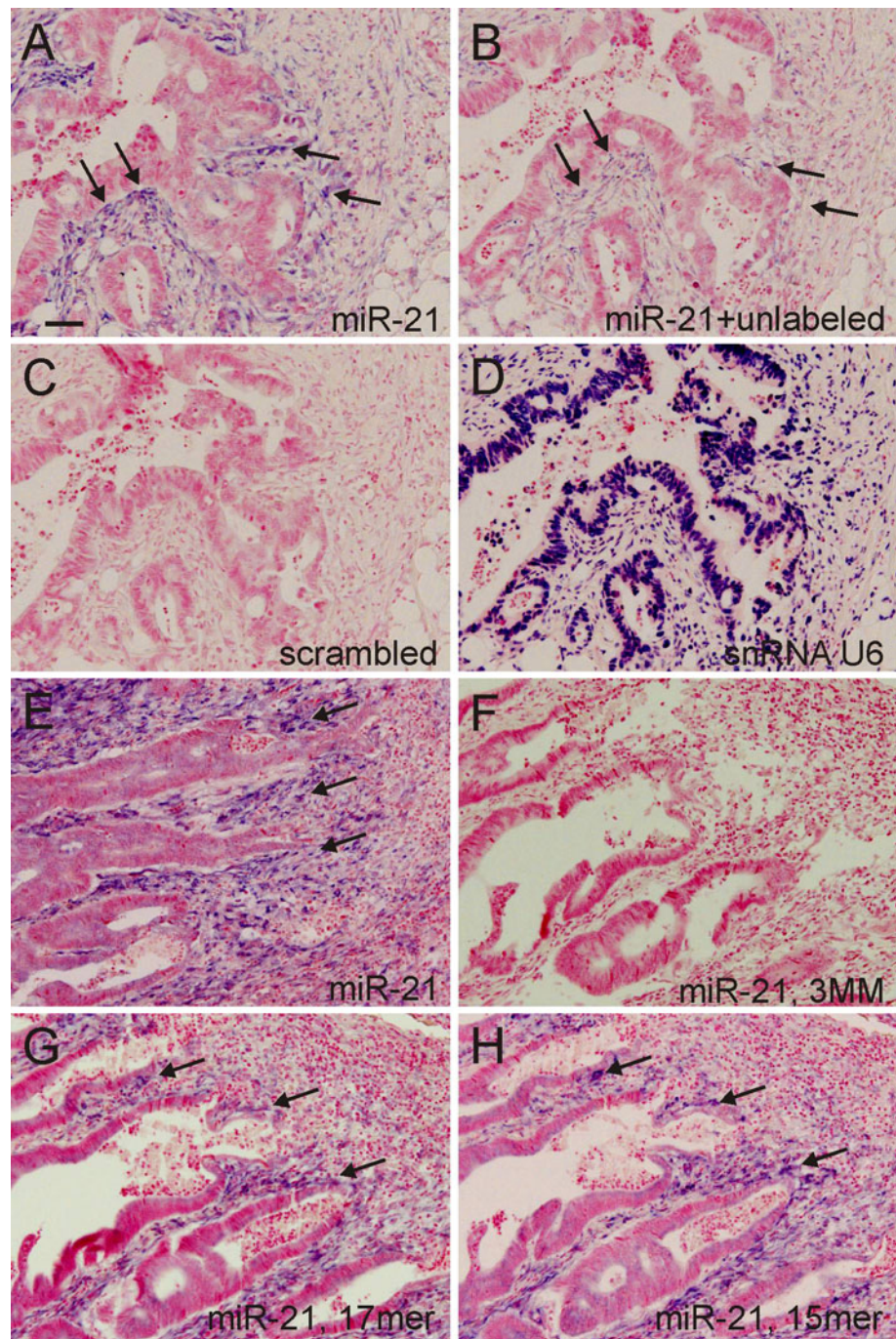
Results

Localization of miR-21 in CRC

For specific identification of miR-21 in tissue sections using ISH, we employed high-affinity LNA-containing DNA oligos labeled at both the 5′- and 3′-ends with DIG. Various hybridization conditions, including tissue pre-digestion, probe concentrations and hybridization temperature were analyzed. Under optimized conditions (see material and methods) we observed strong signal with the double-DIG-labeled miR-21 probe in parallel with little or no background stain, and no signal with the double-DIG-labeled scrambled probe (Fig. 1a, c). Mix-incubating the miR-21 probe with a 2-fold excess of un-labeled probe during hybridization or pre-incubating tissue sections with un-labeled miR-21 probe

Fig. 1 Specificity analysis of miR-21 ISH signal in colon cancer. Four serial tissue sections were obtained from two different colon cancers (**a–d** and **e–h**). Tissue sections were incubated with a full length DIG-labeled LNA probe to miR-21 (**a**), a mix of the DIG-labeled LNA probe to miR-21 (40 nM) together with the un-labeled version of the LNA probe at 80 nM (**b**), DIG-labeled LNA probe with a scrambled sequence (**c**) and a DIG-labeled LNA probe (0.1 nM) specific for snRNA U6 (**d**). Intense miR-21 ISH signal is seen with the miR-21 probe (**a**, *arrows*), while mix-incubating the DIG-labeled miR-21 probe with miR-21 un-labeled oligo strongly reduces the miR-21 ISH signal (compare **a** with **b**). No signal is seen with the DIG-labeled LNA probe having a scrambled sequence (**c**). The snRNA U6 ISH signal is exclusively nuclear in all cells (**d**). Other four serial sections were incubated with double DIG-labeled LNA probes as follows: full length 22-mer miR-21 probe (**e**), a full length miR-21 probe with three mis-matches (**f**), a 17-mer miR-21 probe (**g**), and a 15-mer miR-21 probe (**h**). The three miR-21 probes show an identical hybridization pattern, with intense signal in stromal fibroblast-like cells (**e**, **g**, **h**, examples indicated by arrows). Three mis-matches placed at DNA positions completely prevent hybridization of the probe (**f**). *Bars*: **a–h**: 40 μm


resulted in a strong reduction in the ISH signal (Fig. 1b). ISH signal for snRNA U6 was observed in the nuclei of all cell types (Fig. 1d). Two alternative LNA oligos specific for the miR-21 sequence (17-mer and a 15-mer) showed an ISH pattern identical to the 22-mer full-length probe, whereas a 22-mer miR-21 probe containing three mis-matches showed no staining (Fig. 1e–h).

The miR-21 signal was predominantly observed in the stromal compartment of the CRC (Figs. 1, 2a, b, 4). The intensity varied from case to case and locally within the lesions (Fig. 1a), although there was generally an abrupt decrease of expression at the invasive front. Some cases, approximately 20% (4/22), showed focal expression in cancer cells as clusters within central tumor areas (Fig. 2b, d) or in the tumor periphery (Fig. 2c). Only one case (out of the total of 197 CRC cases) showed predominant miR-21 expression in the cancer cells (data not shown), this patient did not experience recurrent disease within the follow-up period. Smooth muscle cells of muscularis externa often showed miR-21 expression where the cancer
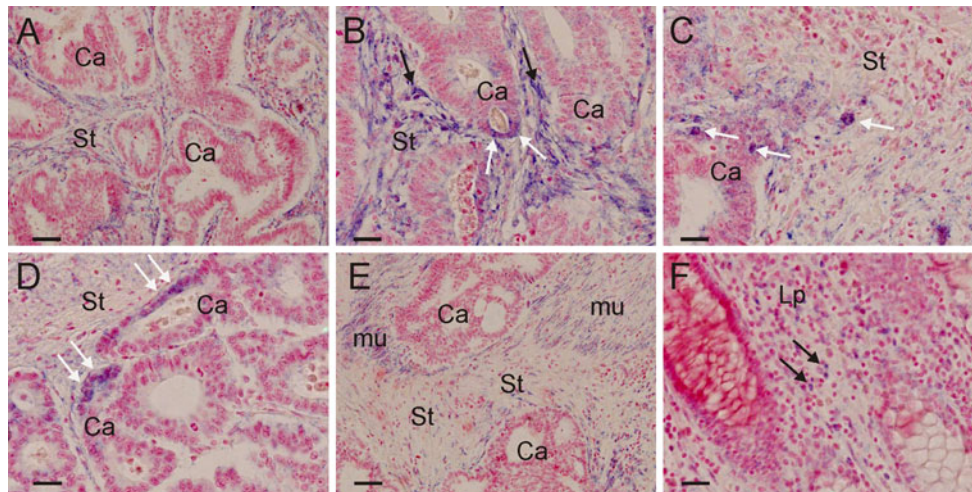
Fig. 2 Localization of miR-21 in colorectal cancers. Tissue sections from colon (**b**, **d**, **f**) and rectal (**a**, **c**, **e**) cancer samples were incubated with a full length DIG-labeled LNA probe to miR-21. Strong miR-21 signal is observed in the stromal compartment (St), predominantly in fibroblast-like cells (**a**, **b**, *black arrows*) in both colon (**b**) and rectal (**a**) cancers. Occasional small clusters of cancer cells are seen within central areas of colon and rectal cancers (**b**, **d**, *white arrows*) as well as at the invasive front (**c**, *arrows*). Weak miR-21 ISH signal is observed in the nearby smooth muscle cells of muscularis externa (indicated by *mu* in **e**). In normal mucosa in proximity to the cancer, a weak ISH signal is seen in a population of lymphocytic cells (**f**, *arrows*) located in lamina propria (Lp). *Bars*: **a**, **b**, **e**: 40 μm, **c**, **d**, **f**: 20 μm

was invading (Fig. 2e), whereas the layer of external smooth muscle under the normal mucosa was miR-21 negative (data not shown). We did not observe any obvious differences in miR-21 expression pattern comparing CC and RC. The miR-21 expression pattern was characterized by intense expression in the tumor area in contrast to the normal mucosa, where weakly stained spherical mononuclear cells were occasionally observed (Fig. 2f). Intense miR-21 ISH signal was also observed in the stromal compartment using fluorescence detection (data not shown). Comparative RT-qPCR was performed on laser capture microdissected colon cancer samples. The levels of miRNA-21 were normalized to the levels of miR-103 and let-7a, which by genome-wide analysis were identified among the most stably expressed miRNAs in these samples. The tumor stromal cells demonstrated 6-fold higher levels ($p < 0.001$) of miR-21 than the cancer cells or normal colon tissue (Fig. 3). We measured an app 2-fold increased expression ($p < 0.05$) in the cancer cell population compared to normal colon tissue. Although this may be explained by minor contamination of miR-21 from adjacent stromal cells, it may also reflect discrete miR-21 expression in cancer cells.
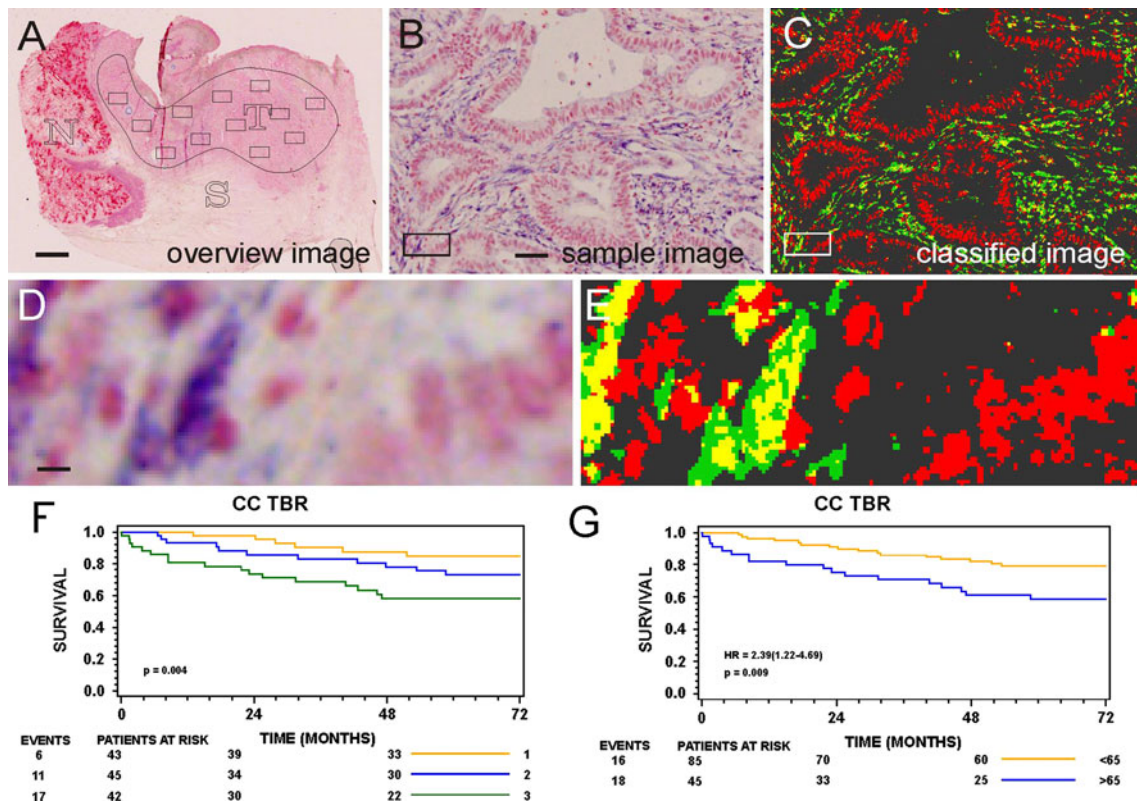
Quantification of the miR-21 ISH signal

Using the optimized ISH conditions, we analyzed the 130 CC and 67 RC cases for the expression of miR-21. Automated ISH allowed uniform incubations across all samples and was used to process two slides from each case for miR-
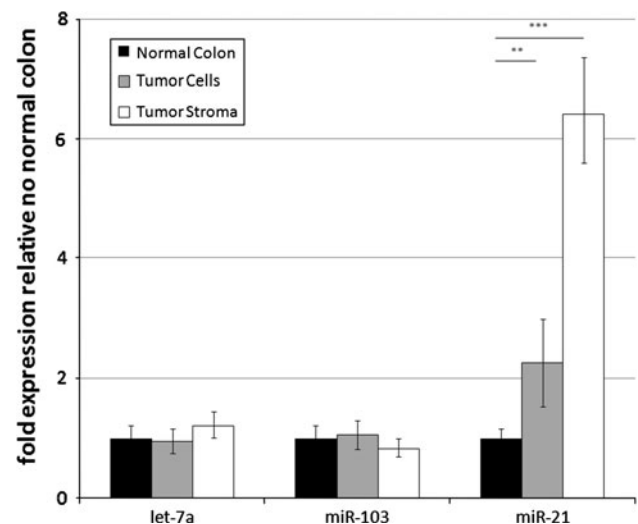
Fig. 3 RT-qPCR for miR-21 in microdissected colon cancer tissue compartments. Areas with colon cancer cells, normal tissue, and tumor stroma were microdissected using LCM. The expression of miRNA-21 was measured by RT-qPCR in duplicate RT and duplicate qPCR for each data point. The levels of miRNA-21 were normalized to the levels of miR-103 and let-7a, which by genome-wide analysis were identified among the most stably expressed miRNAs in these samples. The level of expression in normal colon was set to one and the shown error bars show the standard deviation between determinations (* $p < 0.05$ ($n = 5$, *t*-test), ** $p < 0.001$ ($n = 5$, *t*-test)

21 expression analysis. Since the expression of miR-21 varied considerably within tumors a total of 13 random image fields (median = 13, range 9–33) placed within the tumor area (Fig. 4a) were acquired per patient for subsequent image analysis. Because the expression of miR-21

Fig. 4 Image analysis for quantification of miR-21 ISH signal and Kaplan–Meier estimates of the miR-21 levels to DFS. Typical example of a whole tissue section (a) with normal mucosa (N), tumor area (T) and submucosa (S) after ISH for miR-21 and counterstaining with nuclear red. The tumor area is encircled and random systematically placed image positions are indicated by squared frames (**a**). The sample images are captured with a $20\times$ objective (**b**), which are processed with a supervised pixel classifier separating the *blue* ISH signal, the *red* counter stain, and the *purple* ISH signal overlaying the nuclear *red* (**c**). The area within the frames situated in the lower left corner of (**b**) and (**c**) are in enhanced in (**d**) and (**e**), respectively, to show the conversion of the *blue* ISH signal (**d**) into *green* (**e**), *purple* (**d**) into *yellow* (**e**) and *red* (**d**) into *red* (**e**) in the classified image. Kaplan–Meier estimates of DFS probabilities for miR-21 ISH expression levels measured as TBR values obtained for the 130 colon cancers grouped by their tertiles **f**. The upper tertile with highest miR-21 levels (*green*), the middle tertile with intermediate miR-21 levels (*blue*), and the lower tertile with lowest miR-21 levels (*orange*). Using a cut-point separating the 35% patients with the highest miR-21 levels (*blue* curve in **g**) from those with the lowest (*orange* curve in **g**). The number of patients at risk at time 0, 24 and 48 months for each stratum is shown below the axis and the number of events is shown to the left. *P*-values were obtained using log-rank statistics. *Bars*. **a**: 250 μm, **b–c**: 40 μm, **d–e**: 4 μm

varied according to the number (and density) of positive cells we made the simple assumption that the area covered by the blue ISH signal corresponded to the relative miR-21 expression level. Thus, based on a Bayesian pixel classifier we determined the area of the blue ISH signal, termed B (Fig. 4b, c). We also determined the area of the nuclear red stain (R), as well as the purple area (P) representing the blue ISH signal overlapping with nuclear red (Fig. 4d, e). The following area parameters were obtained: B, R, P, TB (B + P), TR (R + P), and TBR (TB/TR), of which TB and TBR were included in the statistical analyses. Both TB and TBR values represent a relative miR-21 expression level, of which TBR represents values normalized to the nuclear density.

Focal expression of miR-21 throughout tumor areas together with random positioning of image fields caused a considerable variation within slides (125%). However, the precision of the average measures was sufficiently high, giving CV = 67% for TBR values and CV = 71% for TB values within individuals, in comparison with the CVs between individuals, which were 245 and 275%, respectively. The calculated ICCs (the variation for individuals versus the entire variation) were 84% for both TBR and TB values.

The descriptive statistics for the miR-21 quantifications in the CC and RC groups are shown in Table S1. The miR-21 expression levels, measured as TB or TBR values, were similar in the CC and RC patient groups.

Association of miR-21 to clinical characteristics

Comparison with other clinical parameters showed that the male patient group had significantly higher TBR values than the females (Table 1). However, this difference was

Table 1 Correlation analyses of miR-21 expression levels measured as TBR to available clinical parameters for the colorectal cancer patients

Clinical parameter	n	Percentage	miR-21 TBR	P value
Gender				
F	84	43	0.075 (0.002–1.614)	0.034
M	113	57	0.127 (0.002–2.110)	
Localization				
C	130	66	0.100 (0.003–1.619)	0.86
R	67	34	0.1158 (0.002–2.110)	
Age range				
<70	91	46	0.115 (0.002–2.110)	0.62
70–80	80	41	0.114 (0.002–1.104)	
>80	26	13	0.076 (0.011–1.619)	
Grade[a]				
–	18	14	0.065 (0.003–0.536)	0.46
1	4	3	0.252 (0.084–0.533)	
2	101	78	0.116 (0.004–1.619)	
2–3/3	7	5	0.104 (0.004–0.692)	
Type[b]				
A	114	86	0.116 (0.004–1.619)	0.10
M	15	12	0.070 (0.003–0.284)	
S	1	1	0.059	
Total leukocyte count[c]	196	100	$R = 0.09$[e]	0.21
K-RAS[d]				
WT	127	64	0.115 (0.004–2.110)	0.29
Mutation	60	30	0.104 (0.002–1.620)	
MSI[d]				
0	147	74	0.108 (0.002–2.110)	0.85
1	39	20	0.104 (0.004–0.692)	

[a] Differentiation grade, available for the 130 colon cancers cases only

[b] Tumor type available for the 130 colon cancers cases only. *A* adenocarcinomas, *M* mucinous. carcinomas, *S* signet ring carcinomas

[c] data from one colon cancer was not available

[d] PCR data not available in 10 cases (K-RAS) and 11 cases (MSI)

[e] Spearman rank correlation coefficient

not supported by the TB values (Table S2). None of the other clinical parameters (age, grade, type, total leukocyte count, MSI, K-RAS) revealed any correlation with miR-21 expression levels measured as TBR and TB values.

Association of miR-21 to disease-free and overall survival

For the patient cohort, the median follow-up time was at least 60 months and the number of relapses was 34 and 29, the number of deaths 62 and 34 among the CC and RC patients, respectively. The CC patients with high miR-21

expression levels (TBR, $\log_2$-transformed values) had significantly shorter DFS (HR = 1.28, 95% CI: 1.06–1.55, $p = 0.004$) and a higher overall death rate (OS, HR = 1.17, 95% CI: 1.02–1.34, $p = 0.03$). Kaplan–Meier estimates of DFS probabilities for TBR are shown in Fig. 4f, g and for the TB values shown in Fig. S1A. The Kaplan–Meier estimates for TBR (Fig. 4f) and TB values (Fig. S1A) are virtually identical. Considering DFS, the 33% patients with the highest miR-21 TBR-levels, 73% (95% CI: 60–87%) were alive 2 years after surgery, whereas the same rate was 98% (95% CI: 93–100) among the patient tertile with the lowest miR-21 levels. For the middle tertile this number was 86% (95% CI: 75–965). The Kaplan–Meier estimate of the TBR-levels using the 65th percentile as cut-point (corresponding to an expected recurrence rate of 25% adding a 10% margin) is shown in Fig. 4g, and results in a HR of 2.39 (95% CI: 1.22–4.69) for the high-risk population.

Correlation between miR-21 levels and DFS or OS was not observed in the RC group (DFS, HR = 0.96, 95% CI: 0.81–1.15, $p = 0.67$ and OS, HR = 0.97, 95% CI: 0.83–1.13, $p = 0.71$), Fig. S1B, S1C.

Multivariate analysis

Multivariate Cox regression analyses of the DFS data were performed to compare the statistical power of the measured miR-21 expression levels, TBR and TB, and their potential correlations to gender, age and total leukocyte count. Both TB and TBR values were found to be independent predictors of DFS in the CC patient group ($p < 0.05$), Table 2. Including the other clinical parameters (differentiation

Table 2 Multivariate Cox analysis on DFS related to miR-21 expression levels measured as TBR (A) and TB (B) combined with other clinical parameters, gender, age and total leukocyte count (TLC). The TLC value was not available for one colon cancer

A	CC ($n = 129$)			RC ($n = 67$)		
	p value	HR	CI	p value	HR	CI
TBR	0.017	1.261	1.042–1.528	0.7137	0.968	0.816–1.150
Gender	0.338	0.695	0.329–1.464	0.8501	0.929	0.433–1.994
Age	0.914	1.002	0.968–1.037	0.3115	1.018	0.984–1.053
TLC	0.982	1.000	0.998–1.002	0.8860	1.000	0.997–1.002

B	CC ($n = 129$)			RC ($n = 67$)		
	p value	HR	CI	p value	HR	CI
TB	0.012	1.285	1.057–1.562	0.0586	0.854	0.726–1.006
Gender	0.313	0.682	0.324–1.434	0.9858	0.993	0.465–2.120
Age	0.544	1.011	0.975–1.049	0.3034	1.019	0.983–1.055
TLC	0.975	1.000	0.998–1.002	0.9564	1.000	0.997–1.003

grade, tumor type, K-RAS and MSI) in a multivariate model with TBR (CC) resulted in $p = 0.66$, $p = 0.71$, $p = 0.70$, $p = 0.16$, respectively.

Discussion

In the present study we show that a high expression level of miR-21 measured by quantitation of chromogenic ISH signal is associated with short DFS and OS in stage II CC patients. The relative miR-21 expression estimates were found to be independent of other clinical parameters including age, gender, K-RAS and MSI status. We found an intense and well-defined miR-21 ISH signal in the stromal compartment of the tumors using three distinct high affinity antisense LNA probes against the mature miRNA. This localization was supported by RT-qPCR analysis of LCM tissue compartments identifying a 6-fold higher miR-21 level in the stromal compartment compared to that in the cancer cell compartments. The formation of ISH signal was strongly reduced by mix-incubating excess un-labeled probe with the DIG-labeled miR-21 probe on the tissue sections. In addition, no specific ISH signal was observed with two negative control DIG-labeled oligos, one similar to the full-length miR-21 oligo but containing three mis-matches and one with a scrambled sequence. Based on these specificity tests, we conclude that the ISH signal observed represented the presence of genuine miR-21. Taken together, our findings suggest that miR-21 derived from the stromal cell population contributes to the hostile malignant properties of the primary CCs.

The stromal miR-21 positive cells observed in the CRC were generally fibroblast-like in morphology. Cancer associated fibroblasts constitute a heterogeneous cell population with significant growth-promoting impact on tumor progression [32, 33]. Most cancer-associated fibroblasts are myo-differentiated so-called myofibroblasts that may derive from one or more local cell populations like pericryptal myofibroblasts, quiescent interstitial fibroblasts, smooth muscle cells, circulating fibrocytes, and/or by epithelial-to-mesenchymal transition (EMT) [34–36]. Fibroblasts may act on tumor cells through expression of growth factors, such as TGF-β, and thereby contribute to the survival and proliferation of tumor cells [32]. In addition, a number of extracellular proteases are expressed in myofibroblasts, facilitating tissue remodeling and growth factor activation during tumor growth, for example, well-established prognostic cancer biomarkers like uPA and PAI-1 as well as TIMP-1 and MMP-2 are primarily expressed in cancer associated myofibroblasts [37, 38]. Sempere et al. [26] included CC samples in their study and also found miR-21 signal in both tumor cells and tumor associated fibroblast using a double fluorescence approach. A

prevalent expression of miR-21 in CRC stroma was not reported by Schetter et al. [7] who found discrete ISH signals in the tumor area and described the miR-21 positive cells as tumor cells. Yamamichi et al. [25] used an FITC-labeled LNA oligo and TSA-based amplification and found expression of miR-21 ISH signal primarily in cancer cells but also reported stroma cell expression. The reason for these discrepancies is likely explained by cross-reaction of the oligo to "similar sequences" allowed under suboptimal hybridization conditions. Another possible reason for the discrepancy is linked to the different reagents employed to detect the labeled LNA oligo. It should be noted that in the latter two studies [7, 16] only the scrambled probe was included to support the specificity of the ISH signal observed.

For our study we developed a novel ISH procedure for LNA-based miRNA ISH considering procedures described by others [39–41], but suitable for an automated set-up using a Genepaint instrument [42]. We recently established a manual ISH procedure and confirmed the expression pattern for miR-21 as well as for a number of other miR-NAs in various tissues [43]. For semiquantitative analysis, we employed an unbiased image sampling and analysis approach to replace the manual and more subjective scoring of the histological expression intensities. Using image analysis we obtained quantitative estimates of the ISH signal for miR-21 (TB) as well as the area ratio to the nuclear density (TBR). Both estimates showed that the high levels correlated significantly to short DFS in the CC patient group of which the TBR values provided the best correlation. Adjusting the ISH signal to the cell density provided a lower inter slide variation and may therefore explain the slightly better correlation obtained for TBR. The precision of the TBR and TB estimates for each patient was fairly high compared to the variation among individuals. For both TBR and TB estimates, we obtained high ICC values, 84% for both TBR and TB, confirming that the inter-individual variation was substantially larger than the intra-individual variation and a good indication that the two parameters could be significant biomarkers.

The significant correlation of miR-21 to DFS and OS may prove useful for future development of tests to identify stage II CC patients at risk of disease recurrence. In this study we found that miR-21 correlation to CC DFS was independent of other clinical parameters available for some or all of the patients. Thus, none of the parameters available (including age, gender, total leukocyte count, K-RAS or MSI) for the CC patient group (alone or in combination) correlated with DFS or miR-21 ISH levels. A significant correlation between high miR-21 levels and poor survival in CC patients has also been reported by Schetter et al. [7] These authors isolated RNA from normal tissue and CC tissue from 52 stage II patients and obtained cancer/normal

ratios of miR-21 by qPCR. Recently, Schetter et al. found that combining the miR-21 levels with a mRNA expression score for inflammation (Il-6, IL-8, IL10, IL-12a and NOS2a) allowed an even better prognostication of high risk CC patients [6]. This is an interesting observation, which in addition to enforcing the prognostic value of miR-21, also suggests that the molecular profile of the inflammatory response in CC better reflects the risk than the total leukocyte count available in our patient cohort. Increased miR-21 levels measured by either microarray or qPCR have been shown to correlate with poor prognosis in several other cancer types including NSCLC [10], breast cancer [11, 12], and head-and-neck cancer [44, 45]. It has been demonstrated that the cellular origin of miR-21 is also partly stromal in breast [46] and lung cancers [43]. All these data further demonstrate miR-21 as an inherent cancer associated miRNA with a significant impact on tumor growth and dissemination.

Our quantitative measurements of the miR-21 ISH signal identified a significant correlation to DFS in CC patients but not in the RC group. This could be a result of surgical intervention being different or due to different molecular pathways for cancer invasion and dissemination in the two parts of the intestines. The RC patients included in the present study were all operated before the introduction of the TME (Total Mesorectal Excision) operational procedure [47]. The TME practice is associated with a significantly longer DFS probably due to excision of more malignant tissue and/or lymph nodes [48]. Thus, the surgical procedure of the RC patients in this study is a likely confounding parameter that may have prevented the detection of relations between biological events (here miR-21) and disease progression. It cannot be excluded, however, that also other molecular pathways being specific for the RC could contribute to the observed lack of a significant association between miR-21 and DFS in the RC patients.

The miR-21 promoter contains putative binding sites for AP-1, Ets/PU.1, C/EBPα, NFI, SRF, p53, and STAT3 [16]. Activation of the ERK-MAP kinase pathway, induced for example by TGF-β, leads to AP-1 activation and has been found to be augmented by miR-21 in cardiac fibroblasts [19]. TGF-β is expressed at high levels in CRC and induces fibroblast activation and differentiation into myofibroblasts in model systems [49] as well as in CRC tissue [50] where most fibroblasts are myofibroblasts. The mechanism(s) of action of miR-21 in cancer fibroblasts is not known. In various settings, miR-21 has been reported to affect expression of the transcription factor NF1-B in PMA-stimulated HL60 cells [16], Spry1 in cardiac fibroblasts [19], the tumor suppressor PTEN in hepatocytes and cardiac fibroblasts [22, 23], and the tumor suppressor PDCD4 in a variety of cell lines [17, 51]. The identified mRNA

targets vary according to the particular cell line being analyzed.

We have demonstrated that the prevalent expression of miR-21 in the stromal compartment of CC patients is correlated with short DFS and shorter OS. However, it remains unsolved how the miR-21 positive stromal cells contribute to the malignant characteristics of these tumors and whether the sporadic miR-21 positive epithelial cancer cells are also important. If the stromal cell population is directing tumor progression, how do we then explain the recurrent disease after tumor excision? Is the submucosa already primed for promoting local re-growth or are potential metastatic sites already primed for stimulating growth of un-detected micro-metastases? In this context, the miRNAs are truly playing the role as molecular regulators critical to disease progression. Such central roles in cancer have led miRNAs to be considered attractive novel therapeutic cancer targets, both for inhibiting oncogenic miRNAs or by re-introducing miRNAs lost in cancer [52]. To this end, recently it has been demonstrated that miR-21 is strongly upregulated in cardiac fibroblasts in a murine heart failure model and that silencing the fibroblast-derived miR-21 using miR-21 antagonists can prevent or even cure the functional deterioration [19].

References

1. Ferlay J, Autier P, Boniol M et al (2007) Estimates of the cancer incidence, mortality in Europe in 2006. Ann Oncol 18(3):581–592
2. Jemal A, Siegel R, Ward E et al (2008) Cancer statistics, 2008. CA Cancer J Clin 58(2):71–96
3. Baddi L, Benson A III (2005) Adjuvant therapy in stage II colon cancer: current approaches. Oncologist 10(5):325–331
4. Cai X, Hagedorn CH, Cullen BR (2004) Human microRNAs are processed from capped, polyadenylated transcripts that can also function as mRNAs. RNA 10(12):1957–1966
5. Winter J, Jung S, Keller S et al (2009) Many roads to maturity: microRNA biogenesis pathways and their regulation. Nat Cell Biol 11(3):228–234
6. Schetter AJ, Nguyen GH, Bowman ED et al (2009) Association of inflammation-related and microRNA gene expression with cancer-specific mortality of colon adenocarcinoma. Clin Cancer Res 15(18):5878–5887

7. Schetter AJ, Leung SY, Sohn JJ et al (2008) MicroRNA expression profiles associated with prognosis and therapeutic outcome in colon adenocarcinoma. JAMA 299(4):425–436

8. Mathe EA, Nguyen GH, Bowman ED et al (2009) MicroRNA expression in squamous cell carcinoma and adenocarcinoma of the esophagus: associations with survival. Clin Cancer Res 15(19):6192–6200

9. Chan SH, Wu CW, Li AF et al (2008) miR-21 microRNA expression in human gastric carcinomas and its clinical association. Anticancer Res 28(2A):907–911

10. Markou A, Tsaroucha EG, Kaklamanis L et al (2008) Prognostic value of mature microRNA-21 and microRNA-205 overexpression in non-small cell lung cancer by quantitative real-time RT-PCR. Clin Chem 54(10):1696–1704

11. Yan LX, Huang XF, Shao Q et al (2008) MicroRNA miR-21 overexpression in human breast cancer is associated with advanced clinical stage, lymph node metastasis and patient poor prognosis. RNA 14(11):2348–2360

12. Qian B, Katsaros D, Lu L et al (2009) High miR-21 expression in breast cancer associated with poor disease-free survival in early stage disease and high TGF-beta1. Breast Cancer Res Treat 117(1):131–140

13. Krichevsky AM, Gabriely G (2009) miR-21: a small multifaceted RNA. J Cell Mol Med 13(1):39–53

14. Medina PP, Slack FJ (2008) MicroRNAs and cancer: an overview. Cell Cycle 7(16):2485–2492

15. Volinia S, Calin GA, Liu CG et al (2006) A microRNA expression signature of human solid tumors defines cancer gene targets. Proc Natl Acad Sci USA 103(7):2257–2261

16. Fujita S, Ito T, Mizutani T et al (2008) MiR-21 Gene expression triggered by AP-1 is sustained through a double-negative feedback mechanism. J Mol Biol 378(3):492–504

17. Asangani IA, Rasheed SA, Nikolova DA et al (2008) MicroRNA-21 (miR-21) post-transcriptionally downregulates tumor suppressor Pdcd4 and stimulates invasion, intravasation and metastasis in colorectal cancer. Oncogene 27(15):2128–2136

18. Lu Z, Liu M, Stribinskis V et al (2008) MicroRNA-21 promotes cell transformation by targeting the programmed cell death 4 gene. Oncogene 27(31):4373–4379

19. Thum T, Gross C, Fiedler J et al (2008) MicroRNA-21 contributes to myocardial disease by stimulating MAP kinase signalling in fibroblasts. Nature 456(7224):980–984

20. Sayed D, Rane S, Lypowy J et al (2008) MicroRNA-21 targets Sprouty2 and promotes cellular outgrowths. Mol Biol Cell 19(8):3272–3282

21. Gabriely G, Wurdinger T, Kesari S et al (2008) MicroRNA 21 promotes glioma invasion by targeting matrix metalloproteinase regulators. Mol Cell Biol 28(17):5369–5380

22. Roy S, Khanna S, Hussain SR et al (2009) MicroRNA expression in response to murine myocardial infarction: miR-21 regulates fibroblast metalloprotease-2 via phosphatase and tensin homologue. Cardiovasc Res 82(1):21–29

23. Meng F, Henson R, Wehbe-Janek H et al (2007) MicroRNA-21 regulates expression of the PTEN tumor suppressor gene in human hepatocellular cancer. Gastroenterology 133(2):647–658

24. Pezzolesi MG, Platzer P, Waite KA et al (2008) Differential expression of PTEN-targeting microRNAs miR-19a and miR-21 in Cowden syndrome. Am J Hum Genet 82(5):1141–1149

25. Yamamichi N, Shimomura R, Inada K et al (2009) Locked nucleic acid in situ hybridization analysis of miR-21 expression during colorectal cancer development. Clin Cancer Res 15(12):4009–4016

26. Sempere LF, Preis M, Yezefski T et al (2010) Fluorescence-based codetection with protein markers reveals distinct cellular compartments for altered MicroRNA expression in solid tumors. Clin Cancer Res 16(16):4246–4255

27. Mynster T, Nielsen HJ (2000) The impact of storage time of transfused blood on postoperative infectious complications in rectal cancer surgery. Danish RANX05 Colorectal Cancer Study Group. Scand J Gastroenterol 35(2):212–217

28. Nielsen HJ, Hansen U, Christensen IJ et al (1999) Independent prognostic value of eosinophil and mast cell infiltration in colorectal cancer tissue. J Pathol 189(4):487–495

29. Nash GM, Gimbel M, Shia J et al (2003) Automated, multiplex assay for high-frequency microsatellite instability in colorectal cancer. J Clin Oncol 21(16):3105–3112

30. Braasch DA, Corey DR (2001) Locked nucleic acid (LNA): fine-tuning the recognition of DNA and RNA. Chem Biol 8(1):1–7

31. Suraweera N, Duval A, Reperant M et al (2002) Evaluation of tumor microsatellite instability using five quasimonomorphic mononucleotide repeats and pentaplex PCR. Gastroenterology 123(6):1804–1811

32. Kalluri R, Zeisberg M (2006) Fibroblasts in cancer. Nat Rev Cancer 6(5):392–401

33. Orimo A, Weinberg RA (2007) Heterogeneity of stromal fibroblasts in tumors. Cancer Biol Ther 6(4):618–619

34. Direkze NC, Hodivala-Dilke K, Jeffery R et al (2004) Bone marrow contribution to tumor-associated myofibroblasts and fibroblasts. Cancer Res 64(23):8492–8495

35. Yen TH, Wright NA (2006) The gastrointestinal tract stem cell niche. Stem Cell Rev 2(3):203–212

36. Radisky DC, Kenny PA, Bissell MJ (2007) Fibrosis and cancer: do myofibroblasts come also from epithelial cells via EMT? J Cell Biochem 101(4):830–839

37. Nielsen BS, Rank F, Illemann M et al (2007) Stromal cells associated with early invasive foci in human mammary ductal carcinoma in situ coexpress urokinase and urokinase receptor. Int J Cancer 120(10):2086–2095

38. Holten-Andersen MN, Hansen U, Brunner N et al (2005) Localization of tissue inhibitor of metalloproteinases 1 (TIMP-1) in human colorectal adenoma and adenocarcinoma. Int J Cancer 113(2):198–206

39. Silahtaroglu AN, Nolting D, Dyrskjot L et al (2007) Detection of microRNAs in frozen tissue sections by fluorescence in situ hybridization using locked nucleic acid probes and tyramide signal amplification. Nat Protoc 2(10):2520–2528

40. Kloosterman WP, Wienholds E, De BE et al (2006) In situ detection of miRNAs in animal embryos using LNA-modified oligonucleotide probes. Nat Methods 3(1):27–29

41. Nuovo GJ (2008) In situ detection of precursor and mature microRNAs in paraffin embedded, formalin fixed tissues and cell preparations. Methods 44(1):39–46

42. Yaylaoglu MB, Titmus A, Visel A et al (2005) Comprehensive expression atlas of fibroblast growth factors and their receptors generated by a novel robotic in situ hybridization platform. Dev Dyn 234(2):371–386

43. Jorgensen S, Baker A, Moller S, Nielsen BS (2010) Robust one-day in situ hybridization protocol for detection of microRNA in paraffin samples using LNA probes. Methods. doi:10.1016/j.ymeth.2010.07.002

44. Li J, Huang H, Sun L et al (2009) MiR-21 indicates poor prognosis in tongue squamous cell carcinomas as an apoptosis inhibitor. Clin Cancer Res 15(12):3998–4008

45. Avissar M, McClean MD, Kelsey KT et al (2009) MicroRNA expression in head and neck cancer associates with alcohol consumption and survival. Carcinogenesis 30(12):2059–2063

46. Sempere LF, Christensen M, Silahtaroglu A et al (2007) Altered MicroRNA expression confined to specific epithelial cell subpopulations in breast cancer. Cancer Res 67(24):11612–11620

47. MacFarlane JK, Ryall RD, Heald RJ (1993) Mesorectal excision for rectal cancer. Lancet 341(8843):457–460

48. Havenga K, Enker WE, Norstein J et al (1999) Improved survival and local control after total mesorectal excision or D3 lymphadenectomy in the treatment of primary rectal cancer: an international analysis of 1411 patients. Eur J Surg Oncol 25(4):368–374

49. Ronnov-Jessen L, Petersen OW (1993) Induction of alpha-smooth muscle actin by transforming growth factor-beta 1 in quiescent human breast gland fibroblasts. Implications for myofibroblast generation in breast neoplasia. Lab Invest 68(6):696–707

50. Hawinkels LJ, Verspaget HW, van der Reijden JJ et al (2009) Active TGF-beta1 correlates with myofibroblasts and malignancy in the colorectal adenoma-carcinoma sequence. Cancer Sci 100(4):663–670

51. Talotta F, Cimmino A, Matarazzo MR et al (2009) An autoregulatory loop mediated by miR-21 and PDCD4 controls the AP-1 activity in RAS transformation. Oncogene 28(1):73–84

52. Iorio MV, Croce CM (2009) MicroRNAs in cancer: small molecules with a huge impact. J Clin Oncol 27(34):5848–5856